Subcritical Thermal Convection of Liquid Metals in a Rapidly Rotating Sphere

E. j. Kaplan, N. Schaeffer, J. Vidal, Philippe Cardin

HAL Id: insu-02322081
https://insu.hal.science/insu-02322081

Subcritical Thermal Convection of Liquid Metals in a Rapidly Rotating Sphere

E. J. Kaplan, N. Schaeffer, J. Vidal, and P. Cardin
Univ. Grenoble Alpes, CNRS, ISTerre, F-38000 Grenoble, France

Planetary cores consist of liquid metals (low Prandtl number Pr) that convect as the core cools. Here, we study nonlinear convection in a rotating (low Ekman number Ek) planetary core using a fully 3D direct numerical simulation. Near the critical thermal forcing (Rayleigh number Ra), convection onsets as thermal Rossby waves, but as Ra increases, this state is superseded by one dominated by advection. At moderate rotation, these states (here called the weak branch and strong branch, respectively) are smoothly connected. As the planetary core rotates faster, the smooth transition is replaced by hysteresis cycles and subcriticality until the weak branch disappears entirely and the strong branch onsets in a turbulent state at $\mathrm{Ek} < 10^{-6}$. Here, the strong branch persists even as the thermal forcing drops well below the linear onset of convection ($\mathrm{Ra} = 0.7\mathrm{Ra_{crit}}$ in this study). We highlight the importance of the Reynolds stress, which is required for convection to subsist below the linear onset. In addition, the Péclet number is consistently above 10 in the strong branch. We further note the presence of a strong zonal flow that is nonetheless unimportant to the convective state. Our study suggests that, in the asymptotic regime of rapid rotation relevant for planetary interiors, thermal convection of liquid metals in a sphere onsets through a subcritical bifurcation.

Self-sustaining magnetic fields of terrestrial planets are generated in their liquid metal cores. Left on their own they would decay from Ohmic dissipation, but the slow cooling of the planets drives the convective flows thought to maintain the fields [1]. Numerical models of planetary dynamos [2,3] are widely used to study these strongly nonlinear systems. They solve the Navier-Stokes equation coupled to a temperature equation and to the induction equation that governs the magnetic field. For simplicity, most direct numerical simulations of the dynamos have set the Prandtl number Pr = 1. However, liquid metals have Pr $\lesssim 0.1$ and the nature of their convection differs from Pr = 1 [4–6].

The onset of convection in a full sphere is relevant to the early history of the Earth's [7] or the Moon's [8] core, and has thus received a great deal of attention (e.g., Ref. [9]). A significant thermal forcing is required to overcome the stabilizing rotational constraint and drive convective instabilities [9,10]. At and near this threshold, convection onsets in the form of columnar vortices aligned with the axis of rotation, drifting in the azimuthal direction [10,11]. The nonlinear regime has been extensively studied for Pr = 1 [12]. The Pr $\ll 1$ regime is more difficult to tackle [13], but its nonlinear state was recently described using a quasigeostrophic model, which relies on a two-dimensional description of the axial vorticity. In their simplified model, the authors of Ref. [5] found the first clues of subcritical convection—that is, convection below the linear onset of instability—anticipated by weakly nonlinear theoretical predictions [14,15].

In the present work on the rotating convection problem, we use three-dimensional direct numerical simulations to describe the nature of the weak and strong convective branches, especially when the strong branch becomes

subcritical. We discuss the insights gained from the differences and similarities between the two branches.

Formulation of the model.—We study thermal Boussinesq convection driven by internal heating in a sphere rotating at constant angular velocity $\Omega\hat{\mathbf{z}}$. The acceleration due to gravity is radial and increases linearly, as expected for a constant density medium, $\mathbf{g} = g_0 r\hat{\mathbf{r}}$. The radius of the sphere is r_0. The fluid has a kinematic viscosity ν, thermal diffusivity κ, density ρ, heat capacity at constant pressure C_p, and thermal expansion coefficient α, all of which are constant. We consider a homogeneous internal volumetric heating S.

The dynamic system is nondimensionalized by scaling lengths with r_0, times with r_0^2/ν, and temperature with $\nu S r_0^2/(6\rho C_p \kappa^2)$ [5]. The system is governed by the incompressible Navier-Stokes equation and an advection-diffusion equation of the temperature perturbation,

$$\partial_t \mathbf{u} + (\mathbf{u} \cdot \boldsymbol{\nabla})\mathbf{u} + \frac{2}{\mathrm{Ek}}\hat{\mathbf{z}} \times \mathbf{u} = -\boldsymbol{\nabla}p + \Delta\mathbf{u} + \mathrm{Ra}\,\Theta\mathbf{r}, \quad (1)$$

$$\boldsymbol{\nabla} \cdot \mathbf{u} = 0, \quad (2)$$

$$\partial_t \Theta + \mathbf{u} \cdot \boldsymbol{\nabla}\Theta - \frac{2}{\mathrm{Pr}} r u_r = \frac{1}{\mathrm{Pr}}\Delta\Theta, \quad (3)$$

where $\mathbf{u}$ is the velocity field, p is the modified pressure, which includes the centrifugal potential, and Θ is the temperature perturbation relative to T_s. The dimensionless numbers are the Ekman number $\mathrm{Ek} = \nu/r_0^2\Omega$, the Prandtl number $\mathrm{Pr} = \nu/\kappa$, and the Rayleigh number ($\mathrm{Ra} = \alpha g_0 S r_0^6/6\rho C_p \nu\kappa^2$). At $r = r_0$, the boundary condition for

the velocity is no slip and impenetrable (**u** = **0**) and the temperature is fixed (Θ = 0).

This dynamic system is modeled in a three step process. First, for each set of (Ek, Pr), the linear onset of convection Ra_{crit} and the associated eigenmode are computed precisely by using the SINGE code [16] to find the value of Ra for which the least damped eigenmode of the linearized equations has an almost zero growth rate (see the table in the Supplemental Material [17]). The linear eigenmodes are then used as initial values of fully 3D simulations, which are then run until they reach a statistical equilibrium. Hysteresis cycles and subcriticality are explored by changing the thermal forcing or rescaling the final flow state and evolving the system to its new equilibrium.

The fully three-dimensional simulations are run with our spherical code XSHELLS [18,19]. Most runs employ a form of hyperviscosity affecting only the 20% highest spherical harmonics [20] to speed up computations, but we have checked that this does not alter the solutions. Similarly, careful spatial and temporal convergence checks have been made, and we were surprised to find that the amplitude of the zonal winds (axisymmetric azimuthal flow) is very sensitive to the bulk radial grid spacing, although no sharp gradients were seen. We suspect that the balance between the small viscous stress and the small Reynolds stress requires a high resolution to be computed accurately with second order finite differences. As a result, simulations were run using up to 576 cores for 1152 radial levels and spherical harmonics up to degree 199.

The simulations output several useful diagnostic values over the course of the run. We present the velocity using the dimensionless Péclet number ($Pe = Ur_0/\kappa$), which is the ratio between the rate of advection and the rate of diffusion of the temperature. U is defined by the square root of the volume averaged kinetic energy; the zonal Péclet number (Pe_{zon}) uses only the azimuthal component of the flow averaged in longitude ($m = 0$); the convective Péclet number (Pe_{conv}) uses the $m \neq 0$ velocity. We also use the Nusselt number ($Nu \equiv 1/Pr\,\Theta_c$), which measures the convective heat transfer from the core to the surface. (Θ_c is the temperature at the origin).

Weak and strong branches.—Our studies seek to verify that the subcritical behavior found in the quasigeostrophic approximation [5] is also seen in the fully three-dimensional system, for Ek ∈ $[10^{-7}, 10^{-5}]$ and Pr ∈ $[0.003, 0.1]$.

Our results are summarized in Fig. 1, which shows the Péclet number (Pe) versus the Rayleigh number (Ra) for the simulations we have run. Two branches are clearly visible: a strong branch where Pe is larger than 10 and a weak branch with lower Pe. The advantage of representing the kinetic energies in terms of Pe is that it collapses all of the simulations onto a single scale with a clear divide between the strong and weak branches. A more typical Reynolds number representation sees values of kinetic energy that are in either the weak branch or the strong branch depending on
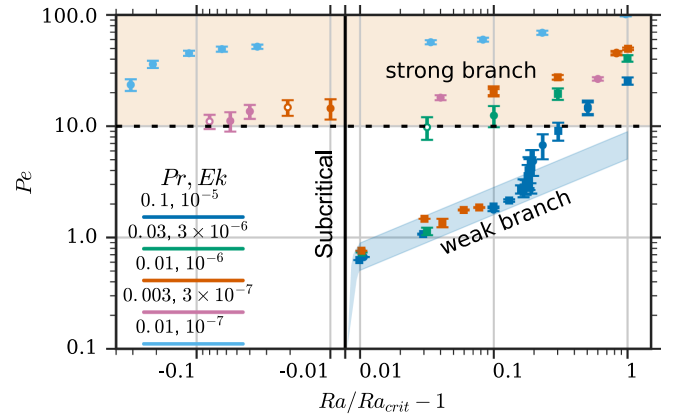

FIG. 1. The mean velocity of the flows as a function of $Ra/Ra_{crit} - 1$. Ek and Pr are indicated by color. The error bars represent fluctuation levels. The open faced markers indicate simulations that were initialized from the strong branch that were observed to either transition to the weak branch, or decay to zero after a finite time greater than τ_κ (the values and fluctuation levels are taken over the time before the transition or decay). The solid black line indicates the onset of the convective instability. The blue parallelogram, indicating the weak branch, scales as $Pe \propto (Ra - Ra_{crit})^{1/2}$ [21].

Pr; an example of this is in Fig. S1 in the Supplemental Material [17]. Pe is also important because one of the markers of the strong branch is a significant cooling of the sphere's core; Pe > 10 indicates that there is enough convective power to draw thermal energy away from the center. At lower Ek, the strong branch persists below the linear critical Rayleigh number.

The weak branch arises from a supercritical bifurcation at Ra_{crit}. For Rayleigh numbers near this value, convection onsets as a thermal Rossby wave [10]. The thermal anomaly Θ in the equatorial plane for a typical case is visible in Fig. 2(a) [13]. The azimuthal velocity v_ϕ in a single meridional slice is shown in Fig. 2(b). The z invariance implied by the quasigeostrophic approximation
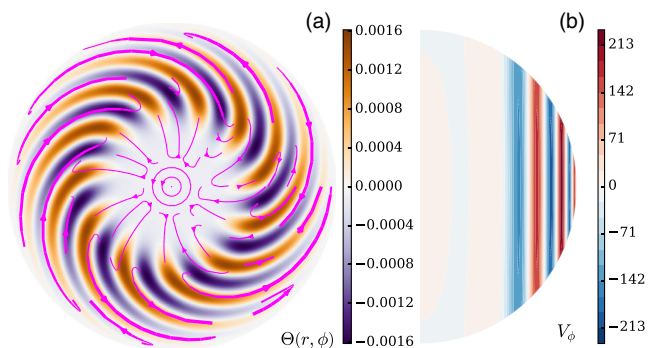

FIG. 2. Cross sections of the weak branch system at Ek = 10^{-6}, Pr = 0.01, Ra = 5.53×10^7 = $1.01\,Ra_{crit}$ showing (a) the temperature profile in the equatorial plane. Streamlines of the flow in the plane are plotted over the temperature profile in pink. (b) Meridional slices of the azimuthal velocity.
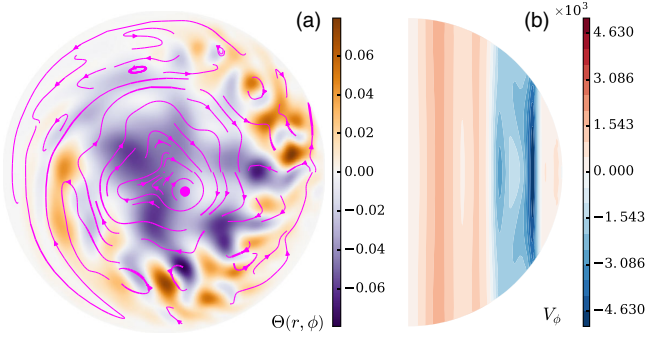
FIG. 3. Same as Fig. 2, but for the strong branch of the system at $Ek = 10^{-6}$, $Pr = 0.01$, $Ra = 5.42 \times 10^7 = 0.99 Ra_{crit}$.

FIG. 4. Phase trajectory of the flow and core temperature for systems at $Pr = 0.03$, $Ek = 3 \times 10^{-6}$, and [(a),(c)] $Ra = 1.03 Ra_{crit}$ and [(b),(d)] $Ra = 1.1 Ra_{crit}$. The top row [(a),(b)] shows runs initialized from a weak branch state; the bottom row [(c),(d)] shows runs initialized from a strong branch state. The lines get darker as the system evolves. The arrows in (a) and (b) indicate the direction of time.

is well displayed. Near onset, the flow driven by the thermal gradient scales roughly with $(Ra - Ra_{crit})^{1/2}$ [21], as shown in Fig. 1.

At large Rayleigh numbers, the weak branch becomes unstable [5] and the flow evolves towards a state where the velocity is an order of magnitude greater. A snapshot of a typical strong branch flow is shown in Fig. 3. The difference with Fig. 2 is stark. There is strong cooling near the origin of the sphere, and a noticeable prograde zonal flow near the axis of rotation. There is some departure from z invariance, but the flow is still mostly columnar.

At $Ek = 10^{-5}$ the strong branch is smoothly connected with the weak branch. Below this Ek the strong branch onsets with a discontinuity, and is characterized by $Pe \gtrsim 10$. This state onsets as a subcritical bifurcation at $Ek \lesssim 3 \times 10^{-6}$, allowing a small hysteresis cycle. The only green open-faced symbol in Fig. 1 represents a simulation that persists in the strong branch for $1.5\tau_\kappa$ ($\tau_\kappa = r_0^2/\kappa$ is the thermal diffusion time) before suddenly decaying to the weak branch. At $Ek = 10^{-6}$ the hysteresis persists below the onset of the weak branch instability.

At lower Ekman numbers ($Ek < 10^{-6}$), the weak branch is absent and the thermal convection operates on the strong branch always at $Pe > 10$. Indeed, we have looked very close above the onset for $Ek = 10^{-7}$ and $Pr = 0.01$: even with an initial perturbation of very low amplitude ($Re \ll 1$) the kinetic energy quickly increased to reach the strong branch. This demonstrates that the saturation mechanism leading to the weak branch at moderate Ekman numbers is lost at higher rotation rates.

The phase trajectories of several simulations at $Pr = 0.03$, $Ek = 3 \times 10^{-6}$ are shown in Fig. 4. A simulation at $Ra = 1.03 Ra_{crit}$, initialized from a weak branch state, is shown in Fig. 4(a). The limit cycle is simple and stable; as the convective power of the flow (indicated by Pe) increases, the core cools (indicated by an increase in Nu), weakening the convection, letting the core heat up again. Figure 4(b) shows a simulation at $Ra = 1.1 Ra_{crit}$, initialized from a weak branch state. The limit cycle here is more complex. The transition to the strong branch happens when other growing modes besides the critical one reach a
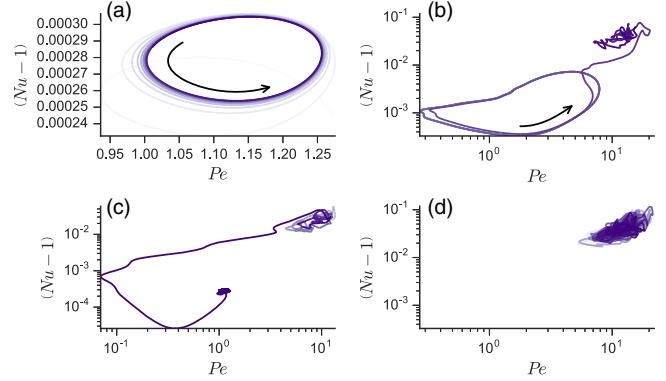
similar amplitude. Simulations at the same two Rayleigh numbers, but initialized in the strong branch, are shown in Figs. 4(c) and 4(d). Here, we see that the phase trajectories are stochastic rather than approaching a limit cycle. At $Ra = 1.03 Ra_{crit}$, the system persists in the strong branch for $1.5\tau_\kappa$ before suddenly jumping to the weak branch. A second observation from Fig. 1 is that the fluctuation levels in the strong branch actually decrease as the thermal forcing is increased. These fluctuations are categorically different from the fluctuations of the weak branch. Here, the fluctuations are stochastic in the phase spaces of the various diagnostic parameters.

Subcriticality.—As Fig. 1 shows, subcritical convection exists in our system, as convection on the strong branch can occur below the linear onset of convection, at $Ra < Ra_{crit}$. Interestingly at $Ek/Pr = 10^{-4}$ the subcriticality is small and fragile: a small perturbation can kick the system back to rest. This is indicated by the open symbols below $Ra < Ra_{crit}$ (Fig. 1), where the flow transitions to rest because of its intrinsic fluctuations, sometimes after several thermal diffusion times.

A much more robust subcriticality is observed at $Ek/Pr = 10^{-5}$ and $Pr = 0.01$. There, the strong branch can be violently perturbed without loosing the convection. As an example, we can divide flow and temperature anomalies by 10 at $Ra = 0.94 Ra_{crit}$ and the convection will quickly recover, while dividing instead by 100 sends the system back to rest. By gradually lowering Ra, we have observed robust convection at decreasing Ra down to $Ra = 0.69 Ra_{crit}$ and have lost the convection at $Ra = 0.64 Ra_{crit}$, when the Péclet number dropped below $Pe \simeq 10$. Further stress tests were applied at $Ra = 0.94 Ra_{crit}$. We artificially removed all $m = 0$ (axisymmetric) components, including the zonal flow and zonal temperature anomaly: the convection stayed firm. We also kept only the most unstable

mode at onset and its harmonics: the convection endured. When removing the $(\mathbf{u} \cdot \boldsymbol{\nabla})\Theta$ term, the kinetic energy increases significantly. Instead, when removing the $(\mathbf{u} \cdot \boldsymbol{\nabla})\mathbf{u}$ term, the subcritical convection dies out.

In the 2D planar geometry studied by Chandrasekhar [4], Veronis predicted a possible subcriticality in a window of low rotation rates [22], recently confirmed numerically [23]. The subcritical behavior is associated with the presence of large mean flows, which reduce locally the effective rate of rotation and, consequently, the rotational constraint on the flow and the critical Rayleigh number toward its nonrotating value. This mechanism implies a Rossby number Ro close to unity. In contrast, it is very small here (Ro $=$ Re $\times$ Ek $< 10^{-3}$) because of the high rotation rate (Ek $= 10^{-7}$) and despite the large Reynolds numbers (Re $\sim 10^{4}$) observed near the convection onset. It is thus not surprising that the zonal flow is not important for subcritical convection. Furthermore, outside the boundary layers and in the subcritical regime, the root-mean-square local vorticity fluctuations never exceed 5% of the background vorticity 2Ω. Not only did Veronis find no subcritical motion in this rapidly rotating regime [24], but the mechanism of lowering the effective (local) rotation rate cannot explain the large amount of subcriticality we found (convection down to Ra $= 0.69$Ra$_{\text{crit}}$).

Our numerical experiments highlight the key role of the Reynolds stress to sustain convection below the linear onset. However, it is the Péclet number that is more conveniently used to characterize the strong branch and subcriticality. If Pe is much larger than 10 at the linear onset [Pe(Ra$_{\text{crit}}$) $\simeq 50$], it is possible to have convection at Ra well below Ra$_{\text{crit}}$, as long as Pe $\gtrsim 10$. Below that threshold, the strong branch of convection cannot survive.

Our study also shows the trend of a lower and lower subcritical Ra/Ra$_{\text{crit}}$ as Ek/Pr is reduced while keeping Pr ~ 0.01. This suggests an even larger effect at planetary core conditions (Ek/Pr $< 10^{-10}$), currently out of reach for numerical models.

Conclusions.—Subcriticality, like hysteresis, implies the presence of active nonlinearities. The zonal flow in this system is produced by nonlinear interaction of the convective velocity (Reynolds stress). In Fig. 5 we plot Pe$_{\text{zon}}$ as a function of Pe$_{\text{conv}}$ over the full set of simulations carried out. The data points seem to align to an inertial scaling law with a power of 3/2 [21]. This scaling law persists not only between the different Ek and Pr, but between the strong and weak branches as well. A set of subcritical runs were rerun with their zonal components artificially canceled (set to zero at every time step) with no significant change in the convective flow or core temperatures. These two factors combined show that the zonal flow is only a byproduct of the convective flows and not a driver of any of the dynamics. This is fundamentally different from the subcriticality predicted for moderate Ekman numbers (Ek ~ 1),
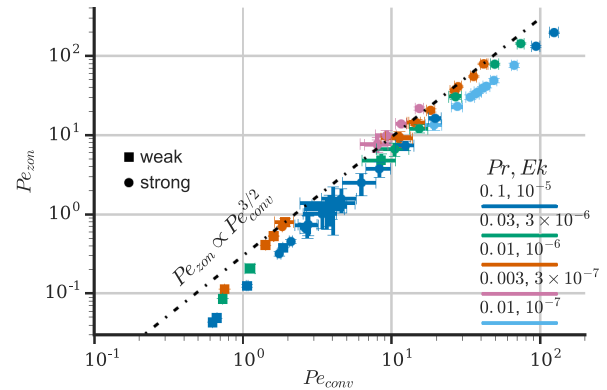

FIG. 5. The averaged zonal velocity Pe$_{\text{zon}}$ of the flows as a function of the averaged convective velocity Pe$_{\text{conv}}$. Ek and Pr are indicated by color. The shape of the markers indicates the branch the averages were taken over. The error bars represent fluctuation levels.

for which the mean flow weakens the stabilizing effect of global rotation [22,23].

[1] C. A. Jones, in *École d'été de Physique des Houches*, edited by P. Cardin and L. Cugliandolo (Elsevier, Amsterdam, 2008), Vol. 88, pp. 45–137.

[2] G. Glatzmaier and P. Roberts, A 3-dimensional self-consistent computer simulation of a geomagnetic reversal, Nature (London) **377**, 203 (1995).

[3] T. Miyagoshi, A. Kageyama, and T. Sato, Zonal flow formation in the Earth's core, Nature (London) **463**, 793 (2010).

[4] S. Chandrasekhar, *Hydrodynamics and Hydrodynamic Stability* (Clarendon, Oxford, 1961).

[5] C. Guervilly and P. Cardin, Subcritical convection of liquid metals in a rotating sphere using a quasi-geostrophic model, J. Fluid Mech. **808**, 61 (2016).

[6] M. A. Calkins, K. Julien, S. M. Tobias, J. M. Aurnou, and P. Marti, Convection-driven kinematic dynamos at low Rossby and magnetic Prandtl numbers: Single mode solutions, Phys. Rev. E **93**, 023115 (2016).

[7] P. Olson, The new core paradox, Science **342**, 431 (2013).

[8] M. Laneuville, M. Wieczorek, D. Breuer, J. Aubert, G. Morard, and T. Rückriemen, A long-lived lunar dynamo

powered by core crystallization, Earth Planet. Sci. Lett. **401,**
251 (2014).

[9] C. A. Jones, A. M. Soward, and A. I. Mussa, The onset of
thermal convection in a rapidly rotating sphere, J. Fluid
Mech. **405,** 157 (2000).

[10] F. H. Busse, Thermal instabilities in rapidly rotating
systems, J. Fluid Mech. **44,** 441 (1970).

[11] E. Dormy, A. M. Soward, C. A. Jones, D. Jault, and P.
Cardin, The onset of thermal convection in rotating spheri-
cal shells, J. Fluid Mech. **501,** 43 (2004).

[12] T. Gastine, J. Wicht, and J. Aubert, Scaling regimes in
spherical shell rotating convection, J. Fluid Mech. **808,** 690
(2016).

[13] K. Zhang, Spiralling columnar convection in rapidly rotat-
ing spherical fluid shells, J. Fluid Mech. **236,** 535 (1992).

[14] A. M. Soward, On the finite amplitude thermal instability of
a rapidly rotating fluid sphere, Geophys. Astrophys. Fluid
Dyn. **9,** 19 (1977).

[15] E. Plaut, Y. Lebranchu, R. Simitev, and F. Busse, Reynolds
stresses and mean fields generated by pure waves: appli-
cations to shear flows and convection in a rotating shell,
J. Fluid Mech. **602,** 303 (2008).

[16] J. Vidal and N. Schaeffer, Quasi-geostrophic modes in the
earth's fluid core with an outer stably stratified layer,
Geophys. J. Int. **202,** 2182 (2015).

[17] See Supplemental Material at http://link.aps.org/
supplemental/10.1103/PhysRevLett.119.094501 for details.

[18] N. Schaeffer, Efficient spherical harmonic transforms aimed
at pseudospectral numerical simulations, Geochem.
Geophys. Geosyst. **14,** 751 (2013).

[19] P. Marti, N. Schaeffer, R. Hollerbach, D. Cébron, C. Nore, F.
Luddens, J.-L. Guermond, J. Aubert, S. Takehiro, Y. Sasaki,
Y.-Y. Hayashi, R. Simitev, F. Busse, S. Vantieghem, and A.
Jackson, Full sphere hydrodynamic and dynamo bench-
marks, Geophys. J. Int. **197,** 119 (2014).

[20] E. Kaplan, H.-C. Nataf, and N. Schaeffer, Dynamic
Domains of DTS: Simulations of a Spherical Magnetized
Couette Flow, arXiv:1610.03964.

[21] N. Gillet and C. A. Jones, The quasi-geostrophic model for
rapidly rotating spherical convection outside the tangent
cylinder, J. Fluid Mech. **554,** 343 (2006).

[22] G. Veronis, Cellular convection with finite amplitude in a
rotating fluid, J. Fluid Mech. **5,** 401 (1959).

[23] C. Beaume, H.-C. Kao, E. Knobloch, and A. Bergeon,
Localized rotating convection with no-slip boundary con-
ditions, Phys. Fluids **25,** 124105 (2013).

[24] G. Veronis, Large-amplitude bénard convection in a rotating
fluid, J. Fluid Mech. **31,** 113 (1968).

[25] https://bitbucket.org/nschaeff/

[26] https://ciment.ujf-grenoble.fr